Supporting Information

Ho et al. 10.1073/pnas.1105189108

SI Supplemental Information

1. Static Contact Angle on Model MgO Surfaces as *D* Decreases. In Fig. 1 of the main text the density profiles are shown for water droplets supported on various surfaces. From the density profiles contact angles were extracted. On MgO the contact angle was found to be approximately 47°, consistent with a hydrophilic surface. When W decreases from 1 to 0 the contact angle increases monotonically because the surface-water interactions become less and less attractive. When W equals 1 but D decreases the contact angle shows a nonmonotonic behavior. Specifically, the contact angle increases from approximately 47° when $D = 1$ to approximately 72° when $D = 0.9$, and then it decreases monotonically as D decreases further. This was unexpected because the surface–water interactions are expected to become more attractive as D decreases, and therefore the contact angle should show a monotonic decrease.

The unexpected result can be explained based on the orientation of the water molecules at contact with the solid substrate, in qualitative agreement with the arguments proposed by Giovambattista et al. (1) and by Lee and Rossky (2), and also by the density of water molecules within the first hydration layer. To quantify these effects we report in Fig. S1 the density profiles for oxygen and hydrogen atoms of water molecules in the direction perpendicular to the solid substrates as D decreases from 1 to 0.62. The results are only shown up to 4 Å from the substrates.

When $D = 1$ (left) the first oxygen peak is found at $z = 2.45$ Å and two hydrogen peaks are found at $z = 1.65$ Å and $z = 3.05$ Å. The first hydrogen peak is closer to the surface than the first oxygen peak, indicating that, on average, one of the OH bonds of about half the water molecules belonging to the first hydration layer points toward the surface. Similar density distributions are found when $D = 0.9$ (second panel from left), suggesting that the orientation of water molecules does not change significantly when D changes from 1 to 0.9. However the oxygen peak is found at $z = 2.65$ Å when $D = 0.9$, farther from the surface than the first oxygen peak on the $D = 1$ surface. The oxygen peak on the $D = 0.9$ surface is also broader and less intense than that on the $D = 1$ surface. These features suggest that interfacial water molecules are, to some extent, repelled from the surface when D is decreased from 1 to 0.9. As a consequence of this molecular-level repulsion the contact angle increases from approximately 47° to approximately 72°, as shown in Fig. 1.

More dramatic are the changes in the density profiles for both oxygen and hydrogen atoms of interfacial water obtained when D is decreased from $D = 0.9$ to $D = 0.7$ (third panel from left) and $D = 0.62$ (right panel). The position of the first O peak is shifted to slightly larger distances from the solid (to $z = 3.05$ Å), but the intensity of the peak increases as D decreases, as a consequence of the increased water-solid attraction due to the enhanced atomic density in the solid substrate. In addition, the first peak for the hydrogen atoms of water becomes centered on the position of the first O peak when $D = 0.7$ or less, and it is slightly more intense than the O peak. This indicates that only a few OH bonds are pointing toward the $D = 0.7$ and $D = 0.62$ surfaces (note the small shoulders near the surfaces in the H density profiles), that more than one OH bonds per water molecule, on average, are approximately parallel to the solid surface, and that the rest are pointing away from the surface. The orientation of interfacial water molecules remains consistent with the description just provided as D decreases from 0.7 to 0.62, but the density of both first O and H peaks at contact with the $D = 0.62$ surface are much larger than those near the $D = 0.7$ surface, as a consequence of the increased surface–water attractions. These changes in the orientation and density of contact water molecules are responsible for the decrease in the equilibrium contact angle found in our simulations as D decreases from 0.9 to lower values.

2. Velocity Profiles in the Couette Flow as a Function of Shear Rate. To assess, in part, how the shear rate affects the results discussed in the main text, we conducted few simulations for selected systems when the shear rate was reduced by half compared to the conditions considered in the main text. The protocol was identical to that described in the main text, with the only difference that the solid surface maintained at a constant velocity was kept at 50 m/s instead of 100 m/s as in the main text. For extensive studies on the effect of shear rate on estimated slip lengths we refer the interested Reader to Refs. 3–5.

In Fig. S2 we report the velocity profiles obtained after the Couette flow was fully established for surfaces with varying W (left panel, $W = 1$, 0.25, and 0) and with varying D (right panel, $D = 1$, 0.7, and 0.62). Note that $W = 1$ and $D = 1$ represent the MgO substrate as obtained by implementing the CLAYFF force field. Qualitatively, the results are consistent with those obtained at higher shear rates (no slip on MgO, hydrodynamic slip on surfaces with $W < 1$, and on surfaces with $D < 0.7$), but the slip length was found to decrease as the shear rate decreases, in qualitative agreement with results by Thompson and Troian (3). To quantify the changes just summarized, in Table S1 we report the slip lengths obtained on two surfaces at the two shear rates considered herein.

3. —Results for the Velocity Profile When $D = 0.7$ and $W = 2$. The Results presented in the main text suggest that the distribution of water molecules within the first hydration layer near a surface is responsible for hydrodynamic slip vs. no slip. However, the strength of surface-water interactions is certainly playing an important role as well. To quantify this effect we chose a surface on which our results show hydrodynamic slip, and we increased the surface-water interactions by enhancing the magnitude of the charges present on the solid atoms by a factor of 2. In the nomenclature used in the present manuscript the surface considered for the present simulation is $W = 2$ and $D = 0.7$.

In Fig. S3 we compare the results obtained on the $W = 1$ $D = 0.7$ and on the $W = 2$ and $D = 0.7$ surfaces. The results considered are contact angles (bottom left panels), velocity profiles after the Couette flow is fully established (top left panel), and density profiles for water molecules within the contact layers (right panels).

Based on the contact angles, our results show that both surfaces are hydrophilic, although the contact angle is lower for the $W = 2$ and $D = 0.7$ (49°) than for the $W = 1$ and $D = 0.7$ (56°) surface.

The velocity profiles show that whereas hydrodynamic slip is observed for the $W = 1$ $D = 0.7$ surface, as described in the main text, hydrodynamic slip significantly decreases and almost disappears when W increases to 2.

The planar density profiles are shown on the $W = 1$ $D = 0.7$ surface and on the $W = 2$ $D = 0.7$ surface at equilibrium (top panels) and after the Couette flow is fully established (bottom panels). As described in the main text, on the $W = 1$ $D = 0.7$ surface the planar density distributions are consistent with the presence of preferential adsorption sites that are found close to each other at equilibrium. Indeed they are so close that when the shear is applied adsorbed water molecules slide from one adsorption site to another yielding well pronounced "density bridges" that connect the various preferential adsorption sites, as described in Fig. 4 of the main text. On the contrary, because of the enhanced surface-water attraction attained when $W = 2$, the planar density distribution at equilibrium shows well defined preferential adsorption sites that are well separated from each other. When shear is applied the planar density distribution is essentially undistinguishable from the one obtained at equilibrium because the water molecules are so strongly bound to their respective adsorption sites that they cannot slide on the surface.

4. Effect of Thermostat on Velocity Profiles. The results discussed in the main text were obtained maintaining the temperature constant for the entire simulated system implementing a Berendsen thermostat in which the velocities of the water molecules were rescaled every time step. To ensure that the results presented do not depend on the thermostat, we repeated selected simulations in which the water temperature was maintained constant at the desired 300 K, but with a Nose-Hoover thermostat (time constant of 100 fs). In Fig. S4 we compare the velocity profiles obtained for water molecules confined between $D = 0.7$ surfaces when the two thermostats are implemented. In agreement with Khare et al.'s expectations (6), we found that the velocity profiles for the confined water molecules do not depend on the algorithm implemented to thermostat the confined water molecules.

1.. Giovambattista N, Debenedetti PG, Rossky PJ (2007) Effect of surface polarity on water contact angle and interfacial hydration structure. *J Phys Chem* 111:9581–9587.

2.. Lee SH, Rossky PJ (1994) A comparison of the structure and dynamics of liquid water at hydrophobic and hydrophilic surfaces—a molecular dynamics simulation study. *J Chem Phys* 100:3334–3345.

3.. Thompson PA, Troian SM (1997) A general boundary condition for liquid flow at solid surfaces. *Nature* 389:360.

4.. Cottin-Bizonne C, Cross B, Steinberger A, Charlaix E (2005) Boundary slip on smooth hydrophobic surfaces: Intrinsic effects and possible artifacts. *Phys Rev Lett* 94:056102–056102.

5.. Martini A, Hsu H-Y, Patankar NA, Lichter S (2008) Slip at high shear rates. *Phys Rev Lett* 100:206001–206001.

6.. Khare R, de Pablo J, Yethiraj A (1997) Molecular simulation and continuum mechanics study of simple fluids in non-isothermal planar couette flows. *J Chem Phys* 107:2589–2596.

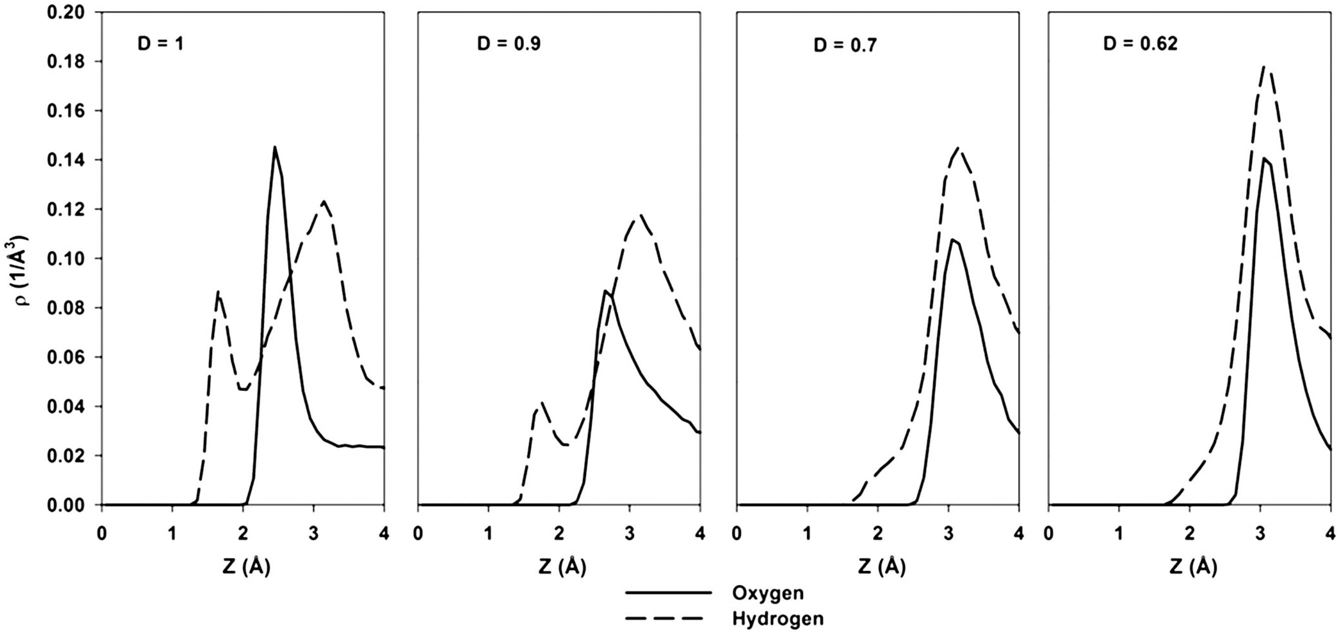

Fig. S1. Density profiles in the direction perpendicular to the solid substrate for oxygen (continuous line) and hydrogen atoms (broken lines) of water molecules within the droplets used to calculate the contact angles of Fig. 1. Results are shown for water on model MgO surfaces in which D decreases from 1 (*Left*) to 0.62 (*Right*). Note that both the intensity and the position of the various peaks change as D changes, reflecting changes in orientation of contact water molecules as well as in the density of the hydration layers.

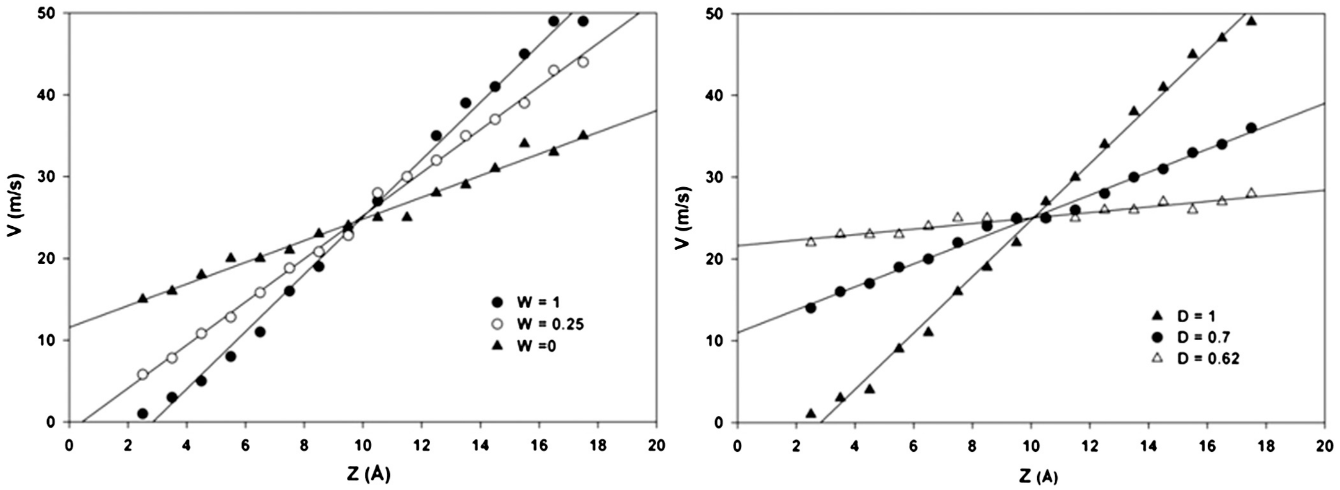

Fig. S2. Velocity profiles obtained after the Couette flow was fully established for water confined in slit-shaped channels. The bottom surface is stationary. The top surface moves with constant velocity of 50 m/s. Results on the *Left* panel are for surfaces of varying *W*. Results on the *Right* panel are for surfaces of varying *D*.

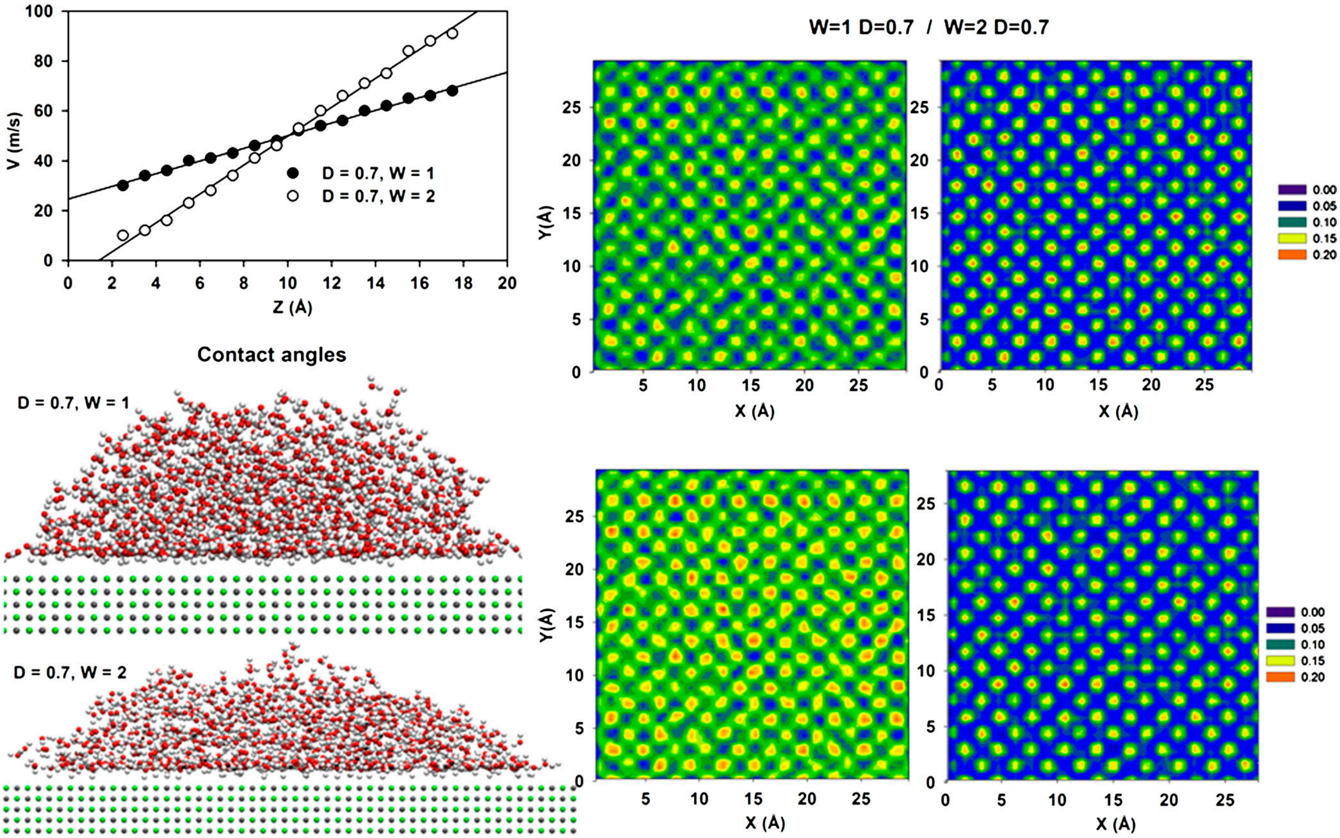

Fig. S3. (*Bottom Left*) Representative simulation snapshots for water droplets supported on model surfaces represented by $W = 2$ $D = 0.7$, and $W = 1$ $D = 0.7$, demonstrating that both surfaces are hydrophilic. (*Top Left*) Velocity profiles obtained for water molecules within slit-shaped channels when the Couette flow is fully established and the confining surfaces are either $W = 1$ $D = 0.7$ (slip) or $W = 2$ $D = 0.7$ (no slip). (*Right*) Planar density profiles at equilibrium (*Upper*) and after the Couette flow is fully established (*Lower*) for water molecules at contact with either the $W = 1$ $D = 0.7$ or the $W = 2$ $D = 0.7$ surface.

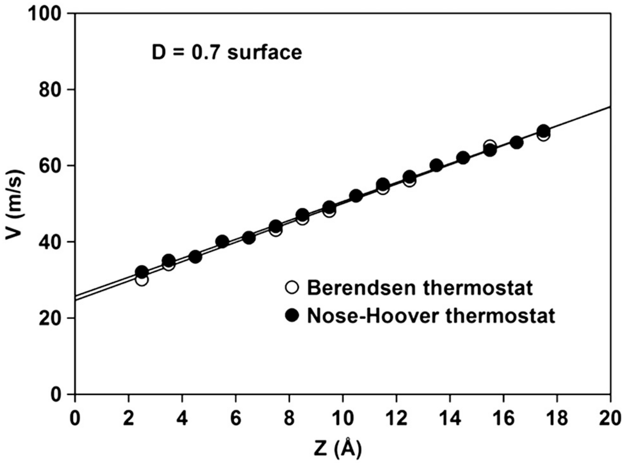

Fig. S4. Velocity profile for water molecules confined within $D = 00.7$ surfaces when the Couette flow of Fig. 2 is fully established. The results are compared when the temperature of the confined water was maintained constant by implementing the Berendsen or the Nose-Hoover thermostat. No appreciable difference was observed. The results in the main text are obtained implementing the Berendsen thermostat and rescaling the velocities of confined water molecules at every time step.

Table S1. Slip length estimated for water on two surfaces ($D = 0.7$ and $W = 0$) as a function of shear rate

Shear rate	$D = 0.7$ surface	$W = 0$ surface
0.5×10^{11} (s^{-1})	9.6 Å	11.2 Å
0.25×10^{11} (s^{-1})	7.7 Å	8.6 Å